Mon. Not. R. Astron. Soc. **000**, 1–8 (2016) Printed 8 August 2016 (MN LATEX style file v2.2)

How unusual is the cool-core radio halo cluster CL1821+643 ?

Ruta Kale [1⋆] and Viral Parekh[2]
[1] *National Centre for Radio Astrophysics, T. I. F. R., Post Bag 3, Ganeshkhind, Pune 411007*
[2] *Raman Research Institute, C. V. Raman Avenue, Sadashivnagar, Bangalore 560080*

8 August 2016

arXiv:1608.01819v1 [astro-ph.CO] 5 Aug 2016

ABSTRACT

Massive galaxy clusters with cool-cores typically host diffuse radio sources called mini-haloes, whereas, those with non-cool-cores host radio haloes. We attempt to understand the unusual nature of the cool-core galaxy cluster CL1821+643 that hosts a Mpc-scale radio halo using new radio observations and morphological analysis of its intra-cluster medium. We present the Giant Metrewave Radio Telescope (GMRT) 610 MHz image of the radio halo. The spectral index, α defined as $S \propto \nu^{-\alpha}$, of the radio halo is 1.0 ± 0.1 over the frequency range of 323 - 610 - 1665 MHz. Archival *Chandra* X-ray data were used to make surface brightness and temperature maps. The morphological parameters Gini, M_{20} and concentration (C) were calculated on X-ray surface brightness maps by including and excluding the central quasar (H1821+643) in the cluster. We find that the cluster CL1821+643, excluding the quasar, is a non-relaxed cluster as seen in the morphological parameter planes. It occupies the same region as other merging radio halo clusters in the temperature- morphology parameter plane. We conclude that this cluster has experienced a non-core-disruptive merger.

Key words: galaxies: clusters: individual (CL1821+643) – radiation mechanisms: non-thermal – X-rays: galaxies: clusters

1 INTRODUCTION

Radio haloes, relics and mini-haloes are terms that refer to diffuse radio sources in clusters of galaxies that are associated with the intra-cluster medium (ICM) as a whole and not with individual galaxies. Such sources are direct probes of the relativistic electrons and magnetic fields in the ICM.

Radio haloes are Mpc-sized diffuse radio sources located nearly cospatially with the X-ray emission from the ICM. Theoretical models invoking reacceleration of seed electrons through a cascade of MHD turbulence introduced in the ICM by merger best explain the observed properties of radio haloes (see Donnert et al. 2013; Brunetti & Jones 2014, for reviews). In addition, relativistic electrons that are secondary products of hadronic interactions in the ICM also contribute but are not sufficient (e. g. Donnert et al. 2010).

Radio mini-haloes are extended sources found surrounding bright central galaxies in cool-core clusters and often bounded by sloshing cold-fronts (e. g. Mazzotta & Giacintucci 2008; Giacintucci et al. 2014b). The origin of mini-haloes has been proposed to be a combination of relativistic electrons produced in hadronic interactions and reaccelerated via MHD turbulence (e. g. Gitti, Brunetti & Setti 2002; ZuHone et al. 2013, 2015).

The occurrence of radio haloes in merging clusters was noticed since the early discoveries of these sources (Giovannini, Tordi & Feretti 1999) and possible scaling relations between the level of disturbance and their power were considered (Buote 2001). Observations of large samples of galaxy clusters have strengthened the scenario that radio haloes nearly exclusively occur in massive and merging clusters and radio mini-haloes in cool-core clusters (Cassano et al. 2010, 2013; Kale et al. 2015).

The recent discovery of a radio halo in the cool-core cluster CL1821+643 challenges the current understanding (Bonafede et al. 2014, hereafter, B14).

1.1 The cluster CL1821+643

CL1821+643 is a massive, $M_{500} = 6.311 \times 10^{14}\ M_{\odot}$ (Planck Collaboration et al. 2014), luminous and rich cool core cluster at a redshift of 0.299 (Schneider et al. 1992). This cluster was discovered surrounding a highly luminous broad-line quasar, namely H1821+643 (Schneider et al. 1992). An FRI type radio source of extent $\sim$ 200 kpc has been found to be associated with the central quasar with possibly precessing jets (Blundell & Rawlings 2001).

⋆ E-mail: ruta@ncra.tifr.res.in

Russell et al. (2010) performed detailed modeling of this quasar using *Chandra* data and were able to subtract the quasar to estimate the internal properties of the cluster itself. They calculated a central radiative cooling time of ~ 1 Gyr which is comparable to other cool core clusters. They also measured a radial temperature decline from 9 keV outside of the central ~ 200 kpc to about 1.3 keV in the core region of 20 kpc. In their X-ray imaging and corresponding temperature map, they noticed elongated morphology of the cluster in the north-west to south-east direction, a few extended arms of emission around the core, an outer swirl with cool gas motion, and a possible cold front generated by the cool-core sloshing. Russell et al. (2010) conclude that the large-scale cluster ICM properties are not substantially affected by the central quasar activity; outside of 8 arcsec (~ 35 kpc), the cluster emission is dominant, and the emission from the quasar is negligible. Recently Walker et al. (2014) analysed thermodynamic properties of the cluster CL1821+643 and found that the entropy around the central quasar between 30 - 80 kpc is substantially lower than that of other comparable massive, strong cool core clusters.

A radio halo of size ~ 1.1 Mpc has been discovered in this cluster at 323 MHz with the GMRT and at 1665 MHz with the VLA D-array by B14. They constrain the spectral index[1] of the radio halo to the range 1.04 - 1.1 over frequencies 323 and 1665 MHz. They used the morphological parameters, Concentration parameter (c), centroid shift (w) and power ratios (P_3/P_0) to characterise its dynamical state based on the X-ray map with archival Chandra data. The cluster is found consistent with relaxed clusters in the $c - P_3/P_0$ plane but is an outlier in the $c - w$ plane due to high w.

In this work we use our GMRT 610 MHz and archival 150 MHz observations to study the radio sources in the cluster. We also perform a morphological parameter analysis of the cluster using a different set of parameters and compare the cluster with a large sample of clusters to understand the peculiarities in this cluster that led it to host a radio halo while still having properties of a cool-core cluster.

We have adopted Λ CDM cosmology with $H_0 = 70$ km s^{-1} Mpc^{-1}, $\Omega_\Lambda = 0.73$ and $\Omega_m = 0.27$. At the redshift 0.299 of the cluster CL1821+643, one arc second corresponds to 4.47 kpc.

2 GMRT OBSERVATIONS AND DATA REDUCTION

The cluster CL1821+643 was observed with the GMRT at 610 and 235 MHz using the dual frequency mode of the GMRT software backend that allows to record one polarization at each frequency band. The data at 235 MHz had to be discarded due to unstable phases on the phase calibrator and high radio frequency interference. The 610 MHz data were recorded with a bandwidth of 32 MHz spread over 512 channels for a duration of 200 min on target source. We used the flagging and calibration pipeline 'FLAGCAL' (Chengalur 2013) for data reduction. This code uses the statistics of median and median absolute deviation for flagging. The flux, bandpass and phase calibrator data are flagged and calibrated first. These are used to calibrate the target source data. The calibrated target source data are flagged and recalibrated if needed. The resulting output FITS file contains flagged and calibrated visibilities on all the sources. These were loaded in NRAO Astronomical Image Processing System (AIPS) for further analysis. The data were first inspected to verify the calibration and flagging. Additional minor flagging was carried out manually. The target source data were then split and averaged in frequency appropriately to reduce the data volume and at the same time avoid being affected by bandwidth smearing. These were then imaged using the AIPS task 'IMAGR' and followed by self-calibration.

Images were produced using the final visibilities with a variety of weighting schemes for the visibilities. The high and low resolution (HR and LR, respectively) images presented in this paper were obtained as follows. The high resolution (HR) image of the point sources in the field was made excluding the visibilities in the inner $2k\lambda$ of the uv-plane and robust= 0. The clean components of the point sources were subtracted from the visibilities using the task 'UVSUB'. The resulting visibilities were used to make a low resolution image of the diffuse emission with robust= 3.0 and uv-distances up to $15k\lambda$. The resulting image was was convolved to a circular beam of $30''$ and is referred to as the low resolution (LR) image.

The amplitude scale is set according to Baars et al. (1977) within the pipeline FLAGCAL used for data analysis. This is converted to the Scaife-Heald 2012 scale using a factor[2] of 1.046 (Scaife & Heald 2012). An amplitude error (σ_{amp}) of 10% is assumed at 610 MHz. The error on the flux density is calculated according to $\Delta S = [(\sigma_{amp}S)^2 + (\sigma_{rms}\sqrt{n_{beams}})^2)]^{1/2}$, where S is the flux density, σ_{rms} is the image rms noise and n_{beams} is the number of beams in the extent of the source.

2.1 Radio Images

The high and low resolution GMRT 610 MHz radio images of the cluster CL1821+643 are presented in Fig. 1. The rms noise in HR and LR images are 0.06 and 0.24 mJy beam^{-1}, respectively. The discrete sources are labelled A and B following the labels used by B14. Source A can be identified with a galaxy SDSS J182154.96+642117.1 and has been classified as a cluster member (Schneider et al. 1992). Source B is an FR I radio source associated with the central quasar H1821+643 (Blundell & Rawlings 2001).

3 X-RAY DATA ANALYSIS AND IMAGES

We used *Chandra* archival data to image the cluster CL1821+643. A summary of the data is given in Table 1. We processed the data with CIAO 4.6 and CALDB 4.6.1.1. The

[1] The spectral index, α is defined as $S_\nu \propto \nu^{-\alpha}$, where S_ν is the flux density at the frequency ν.

[2] The scaling factor of 1.046 given for 750 MHz in Table 7 in Baars et al. (1977) between KPW (Kellermann, Pauliny-Toth & Williams 1969) and Baars 1977 scale is assumed for 610 MHz. Scaife & Heald (2012) use the RCB scale (Roger, Costain & Bridle 1973) for frequencies above 325 MHz which they state is consistent with KPW.

Table 1. CL1821+643 $ChandraACIS-S$ X-ray data.

ObsID, PI	Date of Observation	Exposure time (ks)
9398, A. Fabian	2008-04-21	34.2
9845, A. Fabian	2008-04-14	24.5
9846, A. Fabian	2008-04-20	18.3

Table 2. Radio sources in the CL1821+643 region.

Source	RA_{J2000}	DEC_{J2000}	$S_{610\mathrm{MHz}}$ (mJy)
A	18 21 54.84	+64 21 17.00	110 ± 11
B	18 21 56.99	+64 20 34.99	105 ± 10
Radio Halo	18 21 56.99	+64 20 34.99	35.6 ± 4.0

`chandra_repro` task was used to reprocess all ACIS imaging data. Any high background flares were removed with the task `lc_sigma_clip` (3σ clipping). The read out strip was removed using the `destreak` task, followed by `merge_all` script to combine all data sets. The total exposure time of these combined data is 74.5 ks. All of our event files included the 0.3–7 keV broad energy band and $2''$ pixels binning. We removed point sources around the cluster (except the central bright quasar). We divided counts image with exposure map to generate the flux image. Finally we smoothed this image with $\sigma = 10''$ to remove zero counts. The final images were used to calculate the morphological parameters that serve as proxies to the dynamical state of the cluster.

3.1 Density and temperature maps

Temperature map of the ICM is also a good indicator of the dynamical activity in the cluster. We used XMC (X-ray Monte Carlo) technique to generate it (see Peterson, Marshall & Andersson 2007; Andersson, Peterson & Madejski 2007; Andersson et al. 2009, for details of the method). In this method the spectral and spatial models are used together. We used the warm-absorbed APEC (spectral) model along with the *Chandra* detector (spatial) model derived for XMC. In this analysis, we kept $n_H = 0.0403 \times 10^{22}$ cm^{-2} (Dickey & Lockman 1990), $Z_\odot = 0.3$ and $z = 0.299$ fixed, while allowed temperature (T) to vary between ~ 1 to 15 keV. In this procedure, given (free) parameters (temperature, spatial coordinates of detector, APEC normalisation factor, etc.) of the ICM are iterated using the MCMC technique. The final results have a number of statistical samples of acceptable or converged fits which fall into the "confidence region" of the ICM's input parameters. These well "fitted" parameters describe the properties of the ICM. In this work, all the results derived from the model samples are from the iterations from 500 to 3000, where the value of χ^2 is reduced (to ~ 1) and stable, and is considered to be a converged chain where all corresponding parameters have the best-fitting value. We did not remove quasar from the events file for this analysis. Temperature map shows high value because in the XMC method multi-temperature plasma overlaps on each other which mimics the 'real' situation in ICM plasma (Andersson et al. 2009).

4 RADIO HALO IN CL1821+643

The radio halo is detected at 610 MHz and has an extent of ~ 890 kpc in the north-south and ~ 450 kpc in the east-west direction (Fig. 1, right). The optical image of the cluster field shows the presence of a planetary nebula (PNe) to the northwest of the cluster named, PN G094.0+27.4 associated with the white dwarf WD1821+643 (Fig. 1, left). PNe have spectra of thermal nature that grow weaker at low frequencies with typical strength of a mJy at 1 GHz (e. g. Gurzadyan 1997). No synchrotron emission is known from them though a weak component has been discussed in a few cases (Casassus et al. 2007). Therefore we consider that any contamination from the PNe near the field of this cluster is below our detection limits. The flux density of the radio halo at 610 MHz measured from the low resolution image ($30'' \times 30''$) over the region marked in Fig. 1 (right) is 35.6 ± 4.0 mJy. The spectral index (α) of the radio halo over the frequency range 323 -1665 MHz is 1.0 ± 0.1 (Fig. 2). The k-corrected radio power of the radio halo is $(1.0 \pm 0.1) \times 10^{25}$ W Hz^{-1} according to $P_{610\mathrm{MHz}} = 4\pi d_L^2 S_{610\mathrm{MHz}} (1+z)^{(\alpha-1)}$, where d_L is the luminosity distance.

Magnetic fields in galaxy clusters are ubiquitous and have been observed to be of the order of $\sim 0.1 - 1\mu$G (see Carilli & Taylor 2002; Ferrari et al. 2008, for reviews). It is difficult to measure magnetic fields in clusters directly but can be estimated under assumptions. Assuming equipartition condition, we calculated the magnetic field in the cluster CL1821+643 from the observed radio halo emission. The minimum energy density u_{min} is given by,

$$u_{min}\left[\frac{\mathrm{erg}}{\mathrm{cm}^3}\right] = \xi(\alpha,\nu_1,\nu_2)(1+k)^{4/7}(\nu_{0[\mathrm{MHz}]})^{4\alpha/7} \times (1+z)^{(12+4\alpha)/7}\left(I_{0[\frac{\mathrm{mJy}}{\mathrm{arcsec}^2}]}\right)^{4/7}(d_{[\mathrm{kpc}]})^{-4/7} \quad (1)$$

where k is the ratio of energy in relativistic protons to that in electrons, α is the synchrotron spectral index, ν_0 is the frequency at which the surface brightness, I_0 is measured, d is the depth of the source and $\xi(\alpha,\nu_1,\nu_2)$ is a parameter that is a function of the spectral index and the lower and higher limits in frequency, ν_1 and ν_2 (Govoni & Feretti 2004). The $K-$correction is included and a filling factor of 1 is assumed in the above equation. The magnetic field is then given by,

$$B_{eq[\mathrm{G}]} = \left(\frac{24\pi}{7}u_{min}\right)^{1/2}. \quad (2)$$

The depth of the radio halo was assumed to be the mean of the maximum and minimum extents (890 kpc $\times$450 kpc). The extent in the plane of sky over which the total flux density was measured encloses 22 beams of $30'' \times 30''$ each and thus the surface brightness was calculated to be, 35.6 mJy / ($22\times(30 \times 30$ arcsec^2)). For the $\alpha = 1.0$, $\nu_1 = 10$ MHz and $\nu_2 = 100$GHz, $\xi = 5.39 \times 10^{-13}$. The implied magnetic field under these assumptions is 0.63 μG. The modified equipartition magnetic field (B'_{eq}) based on a limit on the minimum Lorentz factor, $\gamma = 100$ rather than on the frequency (e.g. Beck & Krause 2005), given by,

$$B'_{eq[\mathrm{G}]} \sim 1.1\gamma_{\mathrm{min}}^{\frac{1-2\alpha}{3+\alpha}} B_{eq}^{\frac{7}{2(3+\alpha)}}, \quad (3)$$

where $B_{eq[\mathrm{G}]}$ is from eq. 2, is 1.3 μG for the radio halo.

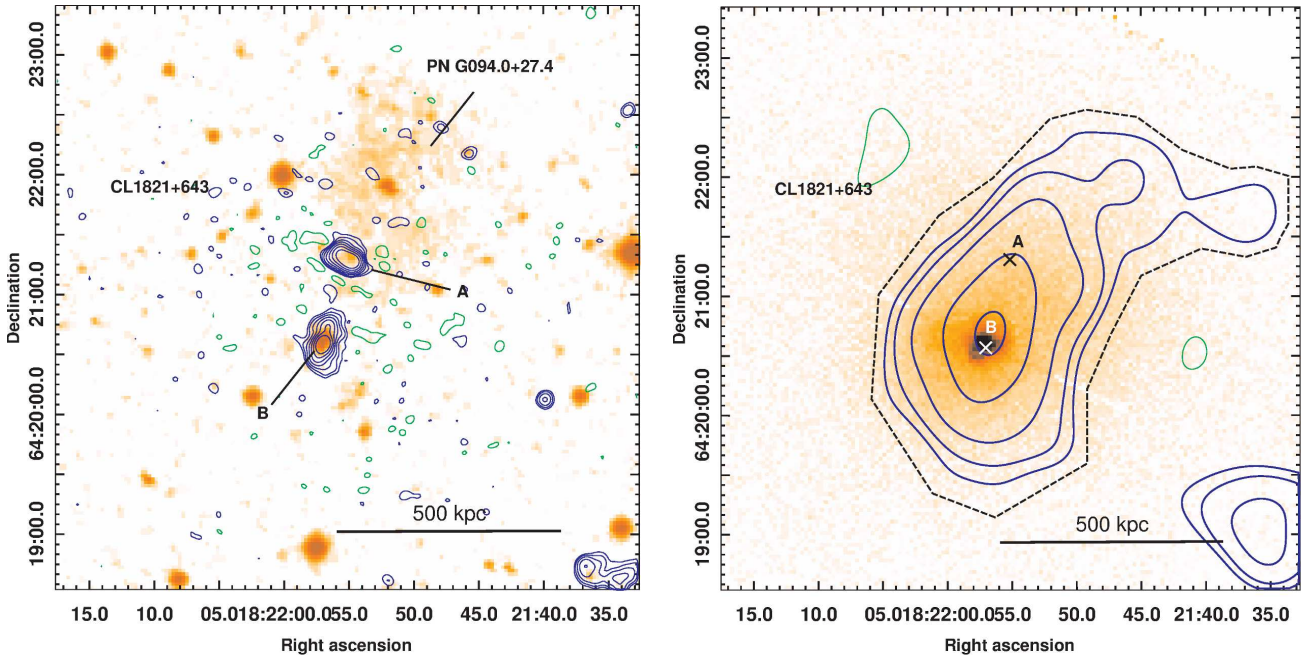

Figure 1. *Left*–GMRT 610 MHz HR image in contours is overlaid on the DSS R-band optical image. The contours are at $0.24\times[-1, 1, 2, 4, ...]$ mJy beam^{-1} and the synthesized beam is $5.1'' \times 5.0''$, p. a. -20.2° . The diffuse emission seen in optical, from the planetary nebula is labelled. *Right*– GMRT 610 MHz LR image shown in contours is overlaid on the Chandra X-ray image in colour. The contour levels are ± 0.9, 1.2, 1.8, 3.0, 4.4 mJy beam^{-1} and the beam is $30'' \times 30''$. The flux density of the radio halo was measured within the region marked by black dashed line. Crosses mark the positions of sources A and B. In both the panels, dark (blue) are +ve and light (green) are -ve contour levels. A colour version of this figure is available online.

5 MORPHOLOGICAL PARAMETERS

The X-ray emitting gas in galaxy clusters carries signatures of dynamical activity that manifests itself as distortions in the X-ray surface brightness images. We computed three morphology parameters, Gini, M_{20} and Concentration (C) using the *Chandra* X-ray image of CL1821+643 to characterise the degree of disturbances in its ICM. These three parameters are known to be effective in seggregating galaxy clusters according to the level of disturbances in them (Parekh et al. 2015, hereafter, P15). Gini is a measure of the flux distribution among the image pixels; its value is 0 if the flux is equally distributed among the pixels and is 1 if most of the flux is contained only in a small number of pixels (Lotz, Primack & Madau 2004). The moment of light, M_{20}, is the normalised second order moment of the relative contribution of the brightest 20% of the pixels (Lotz, Primack & Madau 2004) and is a measure of the spatial distribution of bright cores and substructures in the cluster. The typical values of M_{20} are between -2.5 (very relaxed) to -0.7 (very disturbed) (see P15). The parameter C is a measure of concentration of the flux in the cluster that depends on the ratio of the radii at which 80% and 20% of the cluster flux is found (Conselice 2003) and has a minimum value of 0.0. We point the reader to P15 and the references therein for the details of the parameter calculations.

The parameters for CL1821+643 were calculated with and without the central quasar in order to understand the effect of the quasar on the morphology. For the subtraction of the quasar, we excluded 25 kpc central region around RA 18h21m57.239s DEC +64d20m36.22s similar to that in B14. A flux weighted centre was found in both the cases using an iterative method described in P15. The centres with and without the quasar were found to be separated by 2.83″ which is 13 kpc at the cluster. A region of 500 kpc around the centre was used for the calculation of the morphological parameters. In Table 3 the parameter values along with 1σ uncertainty are stated.

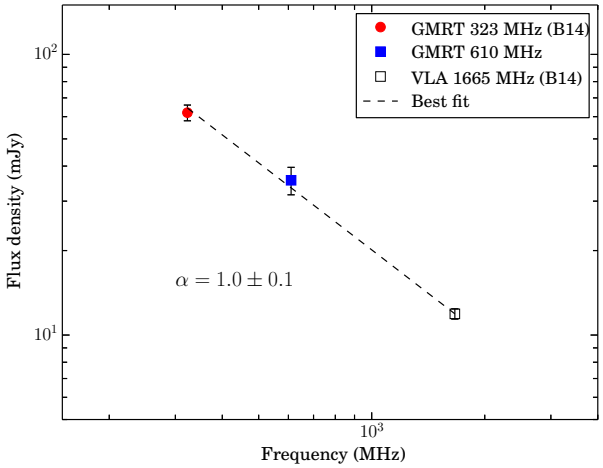

Figure 2. The integrated spectrum of the radio halo in CL1821+643.

Table 3. Morphology parameter values with and without core. The change in the parameter values (percentage) are also given for each parameter in adjacent parentheses.

Cluster	Method	Gini (%change)	M_{20} (%change)	C (%change)
CL1821+643	With quasar	0.66±0.011	-2.17±0.48	1.72±0.51
CL1821+643	Without quasar (25 kpc)	0.58±0.005 (12)	-1.85±0.33 (15)	1.38±0.41 (20)
A2597		0.78 ± 0.0027	-2.42 ±0.25	2.23 ±0.25
A2597	25 kpc core removed	0.75 ± 0.0025 (4)	-2.10 ±0.20 (13)	2.03 ± 0.27 (9)
RXJ1504		0.80 ± 0.0050	-2.47 ± 0.45	2.08 ± 0.35
RXJ1504	25 kpc core removed	0.76 ± 0.0038 (5)	-2.0 ± 0.28 (19)	1.81 ± 0.32 (13)

6 DISCUSSION

The cluster CL1821+643 presents an intriguing case of a radio halo in a cool-core cluster. The properties of the radio halo and the morphological parameters of the cluster are compared with other galaxy clusters with and without radio haloes and those with mini-haloes in order to understand the uniqueness of this cluster.

6.1 Evidence for dynamical activity in CL1821+643

The morphological parameters of galaxy clusters quantify the disturbances in the ICM of the cluster. We compare the parameters calculated for CL1821+643 with a sample of 85 clusters with deep Chandra observations for which morphological parameters are available in P15. Among the sample of 85 clusters, there are 49 low-z (0.2 – 0.3) and 36 high-z (0.3 – 0.8) clusters with X-ray flux, $f > 1.4 \times 10^{-13}$ erg s^{-1} cm^{-2} and $L_X > 3 \times 10^{43}$ erg s^{-1}.

P15 have classified the clusters based on the morphological parameters into four categories of their dynamical states:

Strong Relaxed (SR)
$C > 1.55$, $M_{20} < -2$ and Gini> 0.65;
Relaxed (R)
$1.0 < C < 1.55$, $-2.0 < M_{20} < -1.4$ and $0.40 <$Gini< 0.65;
Non-Relaxed (NR)
$C < 1.0$, $M_{20} > -1.4$ and $0.40 <$Gini< 0.65 and
Strong Non-Relaxed (SNR)
$C < 1.0$, $M_{20} > -1.4$ and Gini< 0.40.

In Fig. 3, the cluster CL1821+643 is shown along with the P15 sample of clusters in the morphological parameter planes.

The SR clusters are well separated from SNR clusters. CL1821+643 with the central quasar falls in the SR cluster category while without the quasar, falls in the NR cluster category. In the first case, all three parameters indicate that CL1821+643 is a relaxed cluster, while in the second case, all three parameters indicate that CL1821+643 is nearly a non-relaxed cluster. This indicates that there are disturbances or substructure present in CL1821+643 outside of the central region, possibly from a high impact parameter merger that kept the central cool-core unaffected.

In the morphological parameter analysis of B14, the parameter, centroid shift showed evidence of dynamical activity and the concentration (a different definition than used in this work) and power ratios implied an undisturbed cluster. The morphological parameters used here show further evidence for the presence of dynamical activity based on the morphology in X-rays. The distribution of galaxies with photometric redshifts between 0.25 - 0.35 selected from the SDSS shows an assymetric distribution around the central quasar (Aravena et al. 2011). This supports the disturbance in the cluster as indicated by the morphological parameters but needs deeper optical studies with spectroscopic identification of cluster members and optical substructure analysis.

6.1.1 Effect of removing the central quasar

The cluster CL1821+643 can be classified as a merging cluster based on the morphological parameters calculated after subtraction of the central quasar. However it is necessary to test if other similar clusters containing bright central sources also turn out to be merging if the central source is removed or they continue to be classified as cool-cores. We selected two strong relaxed clusters, A2597 and RXJ1504 (RXCJ1504-0248) from P15 sample and re-calculated the parameters for these two clusters by removing central 25 kpc region around their peaks in X-rays. These two clusters were chosen for comparison as they are identified as strong relaxed clusters among the P15 sample clusters and their parameter values are similar to the CL1821+643 with the quasar. The parameters and the differences in each are given in Table 3. The change in the parameters when calculated after removing the core is between 12 to 20% in the case of CL1821+643 as compared to 4 to 13% for A2597 and 5 to 19% for RXCJ1504. This excercise illustrates that in CL1821+643 all the three parameters indicate morphological disturbance after removing the central 25 kpc region affected by the quasar. The other two strong cool-core clusters do not show a consistent deviation of morphological parameters towards disturbance after the core is removed. Thus CL1821+643 is different from other cool-core clusters with bright central X-ray sources.

6.1.2 Temperature map and radio halo morphology

The temperature map of CL1821+643 reveals two substructures which appear like 'swirls' (Fig. 4). An inner swirl near the central quasar to the south-west and an outer swirl towards the east of the quasar at a distance of about 130 kpc is seen. The outer swirl is same as that reported by Russell et al. (2010). Such swirls of cold gas have been seen in cool-core clusters and are proposed to be associated with the sloshing of low-entropy gas (Giacintucci et al. 2014a). The radio halo emission extends beyond the swirls but is less extended in the direction perpendicular (east-west) to the swirls as compared to that parallel (north-south) to the swirls (Fig. 4).

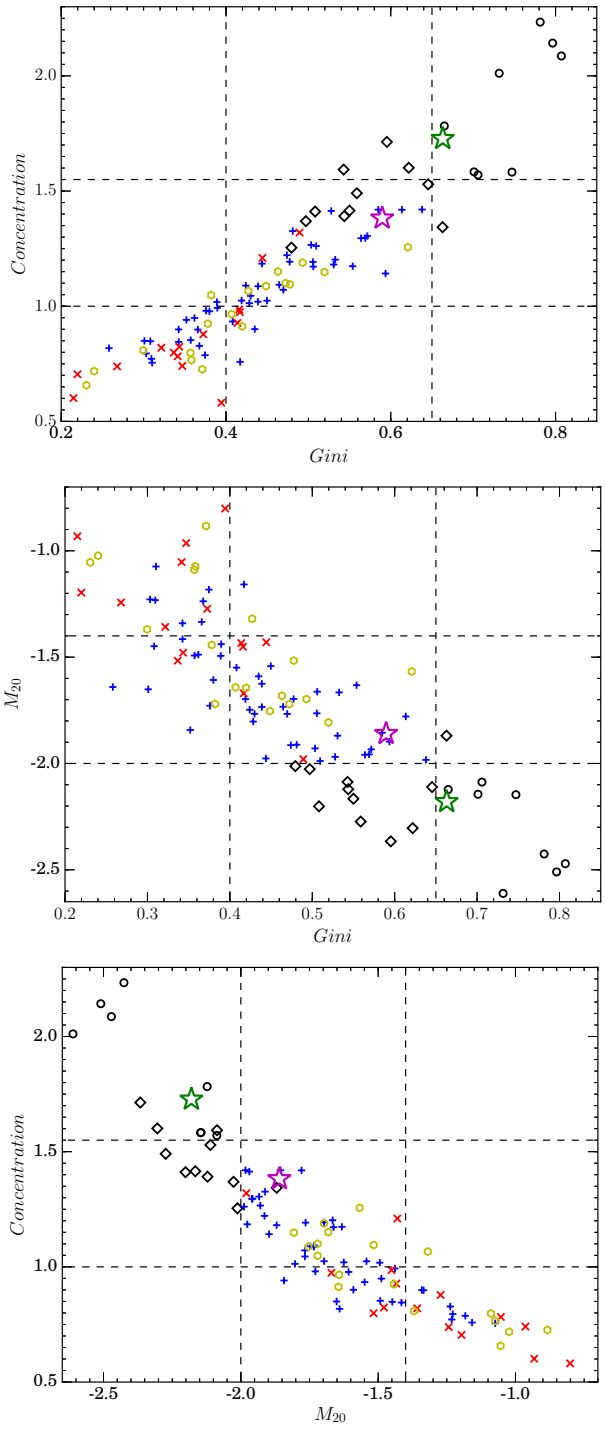

Figure 3. The cluster CL1821+643 is shown in morphology parameter-parameter planes along with the P15 sample of clusters. The green and the magenta stars denote CL1821+643 with and without the central quasar, respectively. The remaining sample clusters are shown according to their classification – circles are 'strong relaxed', diamonds are 'relaxed', plus signs are 'non-relaxed' and crosses are 'strong non-relaxed' clusters. The yellow hexagons are clusters that host radio haloes ($z > 0.1$) taken from (Giovannini et al. 2009) and known to be merging clusters.

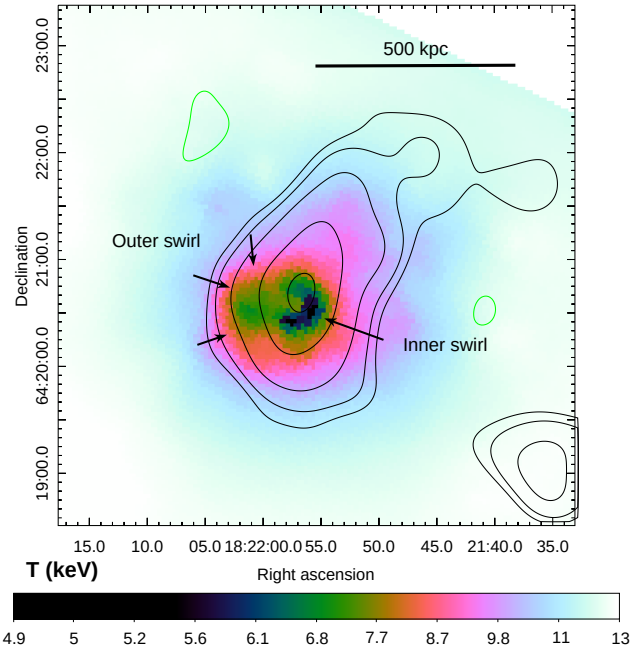

Figure 4. Temperature map shown with the radio halo contours (Fig. 1, right) overlaid. A colour version of the figure is available online.

6.2 CL1821+643 and other clusters with radio haloes

We also compared X-ray morphology of CL1821+643 with that of other clusters with known radio haloes. The morphological parameters (P15) for the sample of radio halo clusters from (Giovannini et al. 2009) with $z > 0.1$ is shown in Fig. 3 (hexagons). The clusters with radio halo are mainly in the NR and SNR categories and CL1821+643 fall in the NR category. It is more relaxed than other radio halo clusters. We analyse the average cluster temperatures of the P15 cluster sample and CL1821+643 in the context of presence of radio haloes. The average temperature of CL1821+643 is 7 kev (B14). CL1821+643 along with P15 and the radio halo sample clusters are plotted in a temperature - morphological parameter plane (Fig. 5). The plane is divided into regions 1, 2 and 3 in which the clusters seggregate. The three regions can also be viewed as an evolutionary sequence of clusters. The SR and R clusters are in region 1 and NR clusters are in region 2 and NR and SNR clusters are in region 3. The region 3 also contains most of the radio halo clusters. This high temperature clusters showing highly disturbed ICM tend to host radio haloes. The cluster CL1821+643 (without quasar) is at the edge of the region 3, implying a disturbed ICM like that of other clusters with radio haloes.

6.3 CL1821+643 and other clusters with mini-haloes

The radio halo in CL1821+643 is under-luminous in radio by a factor ~ 3 as compared to the expectation based on the correlation in the $P_{1.4\mathrm{GHz}} - L_X$ plane for the radio haloes (B14). Since CL1821+643 also shows a cool-core near the quasar, we compare the radio halo with the known mini-haloes. The 1.4 GHz power of the radio halo in CL1821+643, $\log_{10}(P_{1.4\mathrm{GHz}}\mathrm{WHz}^{-1}) = 24.65 \pm 0.05$, was cal-

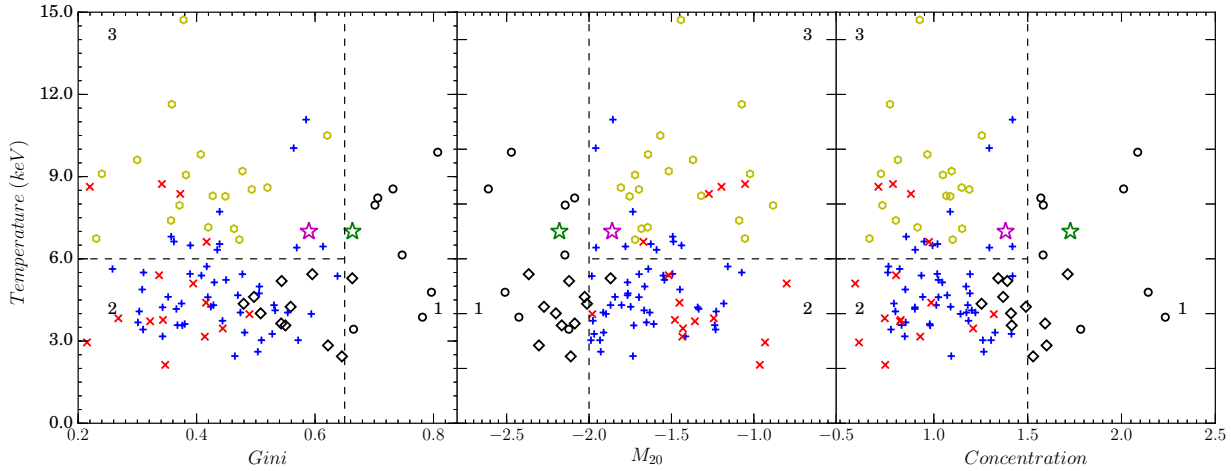

Figure 5. Temperature versus morphological parameters plotted for P15 clusters and CL1821+643. Symbols are the same as Fig.3. The regions marked 1, 2 and 3 indicate the possible evolutionary sequence of a cluster from a strong relaxed cluster to a relaxed cluster and then to a strong non-relaxed cluster. The cluster CL1821+643 without the quasar (magenta star) is located in the region of clusters with radio haloes.

culated assuming a spectral index of 1.0 ± 0.1 between 610 and 1400 MHz. The radio halo in CL1821+643 when plotted with other known mini-haloes in the $P_{1.4\rm GHz} - L_X$ plane appears to be consistent (Fig. 6). The surface brightness of the CL1821+643 is 1.7μJy arcsec^{-2}. Both radio halos and mini-halos with similar surface brightness are known, for example, A1835 and A2254 (Murgia et al. 2009) and it falls in the region of overlap between the haloes and mini-haloes in surface brightness.

This radio halo is unlike other mini-halos that have been found confined to region between 'cold-fronts (e. g. Mazzotta & Giacintucci 2008; Giacintucci et al. 2014a). According to recent MHD simulations the magnetic field structure in the cold-fronts can contain the mini-halo sizes to within the cold-front boundaries leading to a sharp fall in the surface brightness in the direction transverse to the cold-fronts; however allows further expansion in a direction parallel to the cold fronts (ZuHone et al. 2013, 2015). In case of CL1821+643 radio halo is about 450 kpc in width in the direction transverse to the outer cold 'swirl' (Fig. 4) but is nearly two times more in extent in the northwest (see Sec. 6.1.2). The swirls in temperature are similar to cold-fronts(Russell et al. 2010) and the magnetic field in them can prevent further expansion in the transverse direction. The assymetry in the extent of the radio halo may be attributed to the presence of the cold-front-like swirls.

7 CONCLUSIONS

• We have confirmed the radio halo in the cluster CL1821+643 at 610 MHz. Its flux density at 610 MHz is 35.6 ± 4.0 mJy and has an extent of $\sim$ 890 kpc $\times$450 kpc. Equipartition magnetic field estimates of 0.63μG and 1.3μG were obtained under standard assumptions following the methods using low frequency cut-off and low energy (γ_{min}) cut-off, respectively.

• The integrated spectral index of the radio halo is 1.0 ± 0.1 over the frequency range is 323 - 1665 MHz.

• The *Chandra* archival data were reduced to make X-ray surface brightness and temperature maps of CL1821+643. The morphological parameters Concentration (C), Gini and M_{20} were calculated using the surface brightness map and compared with those of a large sample of clusters in P15. CL1821+643 falls in the category of relaxed clusters when the central quasar is included and in that of non-relaxed clusters when the central region was excluded from the morphological analysis.

• CL1821+643 (quasar subtracted) is similar to other clusters with radio haloes in the temperature - morphological parameter plane.

• Being a cool-core cluster with a central quasar, we compared the radio halo with mini-halo clusters. The radio halo in the $P_{1.4\rm GHz} - L_X$ plane for mini-haloes is consistent with other mini-haloes in radio power.

• The larger extent of the radio halo in the north-south direction as compared to that in the east-west may be a consequence of the cosmic ray confinement by the magnetic fields in the cold swirls in the ICM of the cluster as proposed in recent simulations.

ACKNOWLEDGMENTS

We thank the referee for critical comments that improved this paper. RK is supported through the INSPIRE Faculty Award of the Department of Science and Technology (DST), India. We thank the staff of the GMRT, who have made these observations possible. GMRT is run by the National Centre for Radio Astrophysics of the Tata Institute of Fundamental Research. The scientific results reported in this article are based in part on data obtained from the Chandra Data Archive and published previously in cited articles. This research made use of the NASA/IPAC Extragalactic Database (NED), which is operated by the Jet Propulsion

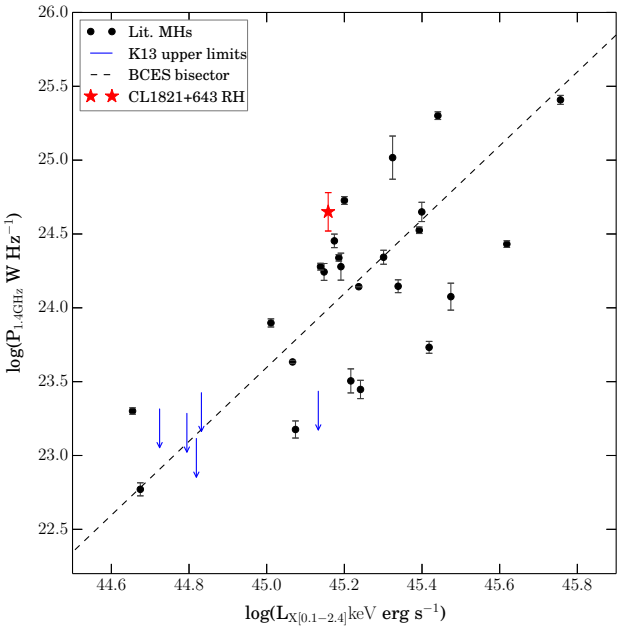

Figure 6. The CL1821+643 radio halo is shown with known mini-haloes in the $P_{1.4\mathrm{GHz}} - L_X$ plane. See Kale et al. (2013, 2015) and references therein for the literature mini-haloes and the upper limits. The best fit line $log(P_{1.4\mathrm{GHz}}) = A \times log(\mathrm{L}_X) + B$ with $A = 2.5 \pm 0.3$ and $B = -88.9 \pm 13.6$ is shown.

Laboratory, California Institute of Technology, under contract with the National Aeronautics and Space Administration. This research made use of data obtained from the High Energy Astrophysics Science Archive Research Center (HEASARC), provided by NASA's Goddard Space Flight Center.

This paper has been typeset from a TEX/ LATEX file prepared by the author.

REFERENCES

Andersson K., Peterson J. R., Madejski G., 2007, ApJ, 670, 1010
Andersson K., Peterson J. R., Madejski G., Goobar A., 2009, ApJ, 696, 1029
Aravena M., Wagg J., Papadopoulos P. P., Feain I. J., 2011, ApJ, 737, 64
Baars J. W. M., Genzel R., Pauliny-Toth I. I. K., Witzel A., 1977, A&A, 61, 99
Beck R., Krause M., 2005, Astronomische Nachrichten, 326, 414
Blundell K. M., Rawlings S., 2001, ApJL, 562, L5
Bonafede A. et al., 2014, MNRAS, 444, L44
Brunetti G., Jones T. W., 2014, International Journal of Modern Physics D, 23, 30007
Buote D. A., 2001, ApJ, 553, L15
Carilli C. L., Taylor G. B., 2002, ARA&A, 40, 319
Casassus S., Nyman L.-Å., Dickinson C., Pearson T. J., 2007, MNRAS, 382, 1607
Cassano R. et al., 2013, ApJ, 777, 141
Cassano R., Ettori S., Giacintucci S., Brunetti G., Markevitch M., Venturi T., Gitti M., 2010, ApJ, 721, L82
Chengalur J. N., 2013, NCRA Technical Report/NCRA/COM/001
Conselice C. J., 2003, ApJS, 147, 1
Dickey J. M., Lockman F. J., 1990, ARA&A, 28, 215
Donnert J., Dolag K., Brunetti G., Cassano R., 2013, MNRAS, 429, 3564
Donnert J., Dolag K., Brunetti G., Cassano R., Bonafede A., 2010, MNRAS, 401, 47
Ferrari C., Govoni F., Schindler S., Bykov A. M., Rephaeli Y., 2008, Space Sci. Rev., 134, 93
Giacintucci S., Markevitch M., Brunetti G., ZuHone J. A., Venturi T., Mazzotta P., Bourdin H., 2014a, ApJ, 795, 73
Giacintucci S., Markevitch M., Venturi T., Clarke T. E., Cassano R., Mazzotta P., 2014b, ApJ, 781, 9
Giovannini G., Bonafede A., Feretti L., Govoni F., Murgia M., Ferrari F., Monti G., 2009, A&A, 507, 1257
Giovannini G., Tordi M., Feretti L., 1999, New Astr. Rev., 4, 141
Gitti M., Brunetti G., Setti G., 2002, A&A, 386, 456
Govoni F., Feretti L., 2004, International Journal of Modern Physics D, 13, 1549
Gurzadyan G. A., 1997, The Physics and Dynamics of Planetary Nebulae. Springer-Verlag Berlin Heidelberg New York.
Kale R. et al., 2015, A&A, 579, A92
Kale R., Venturi T., Giacintucci S., Dallacasa D., Cassano R., Brunetti G., Macario G., Athreya R., 2013, A&A, 557, A99
Kellermann K. I., Pauliny-Toth I. I. K., Williams P. J. S., 1969, ApJ, 157, 1
Lotz J. M., Primack J., Madau P., 2004, AJ, 128, 163
Mazzotta P., Giacintucci S., 2008, ApJ, 675, L9
Murgia M., Govoni F., Markevitch M., Feretti L., Giovannini G., Taylor G. B., Carretti E., 2009, A&A, 499, 679
Parekh V., van der Heyden K., Ferrari C., Angus G., Holwerda B., 2015, A&A, 575, A127
Peterson J. R., Marshall P. J., Andersson K., 2007, ApJ, 655, 109
Planck Collaboration et al., 2014, A&A, 571, A29
Roger R. S., Costain C. H., Bridle A. H., 1973, AJ, 78, 1030
Russell H. R., Sanders J. S., Fabian A. C., Baum S. A., Donahue M., Edge A. C., McNamara B. R., O'Dea C. P., 2010, MNRAS, 406, 1721
Scaife A. M. M., Heald G. H., 2012, MNRAS, 423, L30
Schneider D. P., Bahcall J. N., Gunn J. E., Dressler A., 1992, AJ, 103, 1047
Walker S. A., Fabian A. C., Russell H. R., Sanders J. S., 2014, MNRAS, 442, 2809
ZuHone J. A., Brunetti G., Giacintucci S., Markevitch M., 2015, ApJ, 801, 146
ZuHone J. A., Markevitch M., Brunetti G., Giacintucci S., 2013, ApJ, 762, 78